Experiment and Theory of Bimetallic Pd-Catalyzed α-Arylation and Annulation for Naphthalene Synthesis

Chloe C. Ence, Erin E. Martinez, Samuel R. Himes, S. Hadi Nazari, Mariur Rodriguez Moreno, Manase F. Matu, Samantha G. Larsen, Kyle J. Gassaway, Gabriel A. Valdivia-Berroeta, Stacey J. Smith, Daniel H. Ess,* and David J. Michaelis*

Read Online

ACCESS | Metrics & More | Article Recommendations | SI Supporting Information

ABSTRACT: We report the synthesis of bimetallic Pd(I) and Pd(II) complexes with bidentate 2-phosphinoimidazole ligands and their catalytic activity to generate substituted naphthalenes. This process involves the coupling of an aryl iodide and 2 equiv of a ketone via sequential ketone α-arylation and then annulation to generate disubstituted and tetrasubstituted naphthalenes in a regioselective manner. Excellent substrate scope for both aryl iodide and ketone partners is demonstrated, including that for heteroaryl iodides. Bimetallic Pd complexes are much more reactive than monometallic Pd catalysts in this transformation. Density functional theory calculations, isotope effect experiments, and substrate competition experiments were used to examine bimetallic mechanisms, reactivity, and selectivity.
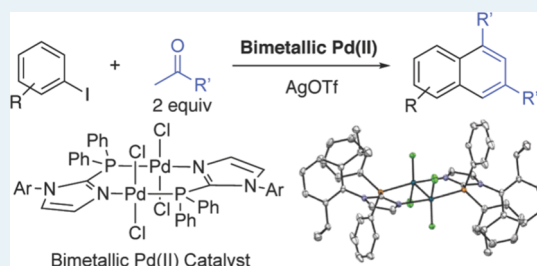
INTRODUCTION

Homo- and heterobimetallic transition metal complexes provide an innovative approach to catalyst development because of the unique reactivity that can result from direct metal−metal bonding cooperativity.[1] A classic example of this type of cooperative benefit is in dirhodium tetracarboxylate catalysis where the presence of a second rhodium center helps facilitate carbene catalysis.[2] More recent examples of bimetallic metal−metal bonding cooperativity in catalysis include Mankad's Cu−Fe-catalyzed arene borylation,[3] Lu's Ni−M hydrogenations,[4] and Uyeda's Ni−Ni cycloaddition reactions,[5] among others.[6] Our groups have also used experiments and theory to understand metal−metal cooperativity in Pd−Ti allylic aminations.[7] Each of these examples of bimetallic catalysis achieves either increased efficiency and selectivity or new reaction mechanisms that cannot generally or easily be accessed with monometallic catalysts.

One potential advantage of having two metals participate in a catalytic process is the opportunity to access less common catalyst oxidation states that enable new types of reactivity and mechanisms.[8] For Pd, examples of accessing less common oxidation states with bimetallic structures include Ritter and Sanford's Pd(II) dimers[9] that can facilitate binuclear oxidative addition to a Pd(III) dimer, which can circumvent forming higher-energy Pd(IV) intermediates (Figure 1a).[10] Hartwig, Schoenebeck, Hazari, and others have also developed a diverse set of lower oxidation state Pd(I) dimer precatalysts that efficiently perform a range of cross-coupling reactions, including Suzuki, Negishi, Sonogashira, and Buchwald−
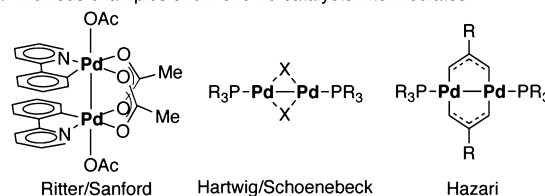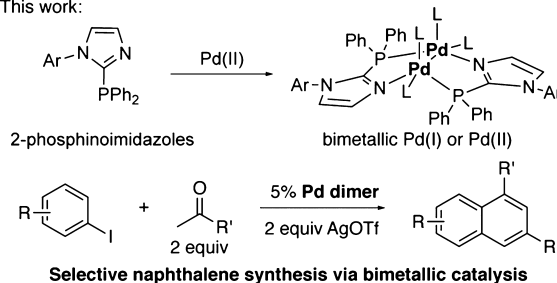
Figure 1. (a) Examples of bimetallic Pd complexes in catalysis. (b) Outline of bimetallic Pd catalysis in this work.

Hartwig amination reactions (Figure 1a).[6,11] Pd(I) dimers can also serve as precatalysts for the α-arylation of ketones and esters, which is relevant to the work presented here.[12] Several recent studies have suggested that Pd(I) dimers can remain intact during catalysis and enable cooperative bimetallic catalysis.[13] For example, Schoenebeck reported catalysis with Pd(I) dimer $[(t\text{-Bu}_3\text{P})\text{PdI}]_2$ that undergoes oxidative addition across the Pd(I)−Pd(I) complex.[13a]

In this work, we report the discovery of a new class of stable and catalytically active bimetallic Pd(I) and Pd(II) complexes with bridging 2-phosphinoimidazole ligands.[14] These new complexes enable a previously unknown sequential ketone α-arylation and annulation reaction that generates high yields of difficult-to-synthesize disubstituted and tetrasubstituted naphthalenes in a single transformation (Figure 1b). The naphthalene products are generated in a regioselective manner across a broad range of iodide and ketone starting materials, including heteroaromatic iodides. While synthetic approaches to 1,3-disubstituted and tetrasubstituted naphthalenes have been demonstrated previously, they generally require multistep syntheses.[15] This new transformation enables direct access to substituted naphthalenes in a single step from commercially available aryl iodides and methyl ketones. Substituted naphthalenes have a variety of technological and pharmacological uses,[16] including as templates to construct carbon nanotubes[17] and as proton-conducting solid electrolytes.[18] Importantly, typical monometallic complexes show no or very little reaction in this new process. Density functional theory (DFT) calculations and isotope effect experiments provide key insights into possible reaction mechanisms and bimetallic reactivity.

RESULTS AND DISCUSSION

We began with the synthesis of new bimetallic Pd complexes generated from 2-diphenylphosphino-1-arylimidazole ligands. We found that the identity of both the ligand and the palladium precursor had a significant impact on the complex obtained. For example, when ligand 1 was mixed with PdCl$_2$ in methanol, only a monomeric Pd complex 2 was obtained, where Pd was inserted between the P−C bond of the ligand (Figure 2a). We recently demonstrated that this new N−H N-heterocyclic carbene−palladium complex is highly active in palladium-catalyzed Suzuki−Miyaura reactions.[19] In contrast, we found that if ligand 1 was first coordinated with a boron Lewis acid to form 3, formation of a bimetallic Pd(II) complex 4 was observed upon addition of PdCl$_2$ in dioxane (Figure 2b). Bimetallic Pd(II) complexes similar to 4 have been previously reported by Manzano but required the use of PdMeCl as a precursor to obtain the bimetallic structure.[14a] Alternatively, if Pd(OAc)$_2$ was employed instead of PdCl$_2$, Pd(I) dimer 5 was obtained. The mechanism for *in situ* reduction of Pd(II) precursors to Pd(I) dimer complexes was recently reported by Schoenebeck and Colacot and likely involves the oxidation of one-third of the phosphine ligand.[20] This mechanism would explain the modest yield of the reaction to form complex 5. We believe that the presence of the boron ligand may help facilitate faster ligand coordination via a transmetalation-like mechanism. For example, when ligand 3 is added to PdCl$_2$, complex 4 is generated in 66% yield after 18 h. However, when ligand 1 is employed, which does not contain the boron Lewis acid, complex 4 is isolated in 43% yield after 3 days in the absence of methanol.
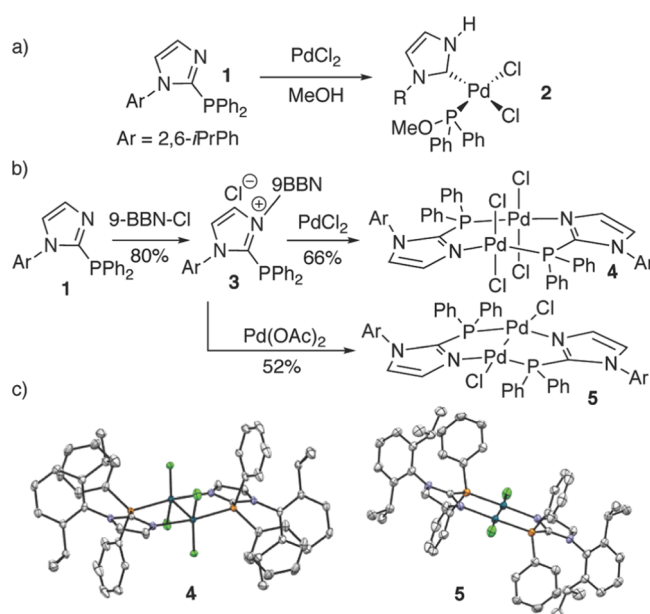

Figure 2. Synthesis and structure of bimetallic Pd complexes.

The crystal structures of these bimetallic Pd complexes provide additional insights into their structure and potential reactivity (Figure 2c). In 4, the two palladium centers are held within the van der Waals contact distance for a Pd−Pd bond (Pd van der Waals radius = ~1.6 Å), but the absence of unpaired electrons prevents Pd−Pd bond formation (Pd−Pd distance = 2.966 Å). The calculated formal shortness ratio (FSR) of 1.16 for complex 4 is close to the limit for covalent metal−metal bonding (FSR limit $\geq$ 1.22, see the Supporting Information).[21] Because the phosphinoimidazole ligand holds the Pd centers in close proximity, there is distortion away from a square planar geometry, likely to mitigate repulsion between the filled d_z^2 orbitals of each Pd. The τ parameter for 4 is 0.16 (0 being square planar and 1 being tetrahedral), which shows moderate distortion away from a perfect square planar geometry.[22]

For Pd(I) dimer 5, the presence of unpaired electrons on each Pd center leads to Pd−Pd bond formation with a distance of 2.591 Å. The square planar geometry of the two palladium centers and their oxidation states are also consistent with metal−metal bond formation. The calculated FSR for complex 5 is 1.01, which represents a significantly higher bond order than that with 4 and is consistent with the formation of a single bond between the two palladiums. The M06 DFT-calculated orbitals for 4 and 5 confirm that 4 lacks direct Pd−Pd covalent bonding and the HOMO consists mainly of antibonding d_z^2 orbitals (Figure 3).[23,24] The HOMO of 5, in contrast, shows a direct Pd−Pd covalent bond.

With two new bimetallic Pd complexes, one with Pd metal centers in close proximity and one with a Pd−Pd covalent bond, we next set out to explore the reactions that could potentially exploit Pd−Pd cooperativity to achieve novel reactivity. We were especially interested in reactions where monometallic Pd catalysts either fail, are very slow, or are unselective. We found that our Pd dimers could enable the generation of 1,3-disubstituted and tetrasubstituted naphthalenes via the coupling of aryl iodides and methyl ketones, which represents a completely new approach to these compounds. Table 1 reports the use of monometallic and
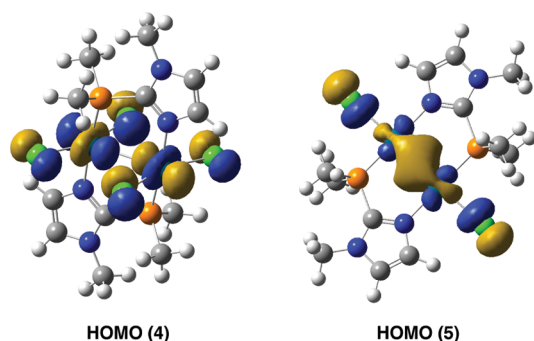
Figure 3. M06/6-31G**[LANL2DZ for Pd]-calculated HOMOs of model complexes for **4** and **5**.[23,24]

Table 1. Optimization of Reaction Conditions

entry[a]	Lewis acid	catalyst	time	% yield[b]
1	AgOTf	PdCl$_2$ + dppe	1 h	NR
2	AgOTf	PdCl$_2$ + BINAP	18 h	NR
3	AgOTf	PdCl$_2$ + DTBM-SEGPHOS	18 h	NR
4	AgOTf	PdCl$_2$ + c-hex-diamine	18 h	NR
5	AgOTf	PdCl$_2$ + PPh$_3$	1 h	28
6	AgOTf	complex **4**	1 h	100 (89)
7	AgOTf	complex **5**	1 h	100 (84)
8	AgOTf	Pd(OAc)$_2$ + **3**	1 h	100 (90)
9	AgOTf	PdCl$_2$ + **3**	1 h	100 (93)
10	CuOTf	PdCl$_2$ + **3**	16 h	85
11	FeOTf	PdCl$_2$ + **3**	16 h	NR
12	AgTFA	PdCl$_2$ + **3**	16 h	NR
13	AgOAc	PdCl$_2$ + **3**	16 h	NR
14	AgOTf	PdCl$_2$ + **1**	1 h	45
15	AgOTf	PdCl$_2$ + ArImid[c]	1 h	NR
16	AgOTf	(PtBu$_3$)$_2$Pd$_2$Br$_2$	1 h	26
17	AgOTf	**3**	1 h	NR
18[d]	AgOTf	PdCl$_2$ + **3**	18 h	NR

[a]Reactions run with 0.5 mmol iodobenzene, 1.25 mmol acetophenone, and 0.025 mmol **4** or **5** or 10% ligand and 10% PdCl$_2$ for *in situ* reactions at 0.5 M in dioxane. [b]Yields determined by ^{1}H NMR analysis of the crude reaction mixture by comparison to an internal standard (isolated yields in parentheses). NR = no reaction. [c]ArImid = N-(2,6-diisopropylphenyl)imidazole. [d]With 2 equiv of TfOH.

bimetallic Pd catalysts for the coupling of phenyl iodide and acetophenone partners to generate naphthalene **6a**. Entries 1–5 show that the use of monometallic Pd catalysts either results in no reaction or less than 30% yield. For example, PdCl$_2$ with dppe resulted in no reaction, and PdCl$_2$ with BINAP, SEGPHOS, or a diamine ligand resulted in no reaction even after 18 h. However, there was a small yield (28%) of product with PdCl$_2$ and PPh$_3$ (entry 5). Additionally, our monometallic Pd catalyst **2** resulted in no reaction (see the Supporting Information). In contrast to the general poor performance of monometallic Pd catalysts, bimetallic catalysts **4** and **5** showed high reactivity. Under our optimized conditions with 2.5 equiv of ketone and 2 equiv of AgOTf in dioxane (optimal solvent, see the Supporting Information) at 80 °C, the reaction proceeded to 100% conversion with bimetallic complexes **4** and **5** and provided 89 and 84% yields of the naphthalene

product, respectively (entries 6 and 7). In addition, we found that simply pre-stirring ligand **3** with PdCl$_2$ or Pd(OAc)$_2$ in dioxane for 15 min led to the formation of bimetallic complexes **4** and **5**, respectively, as observed by ^{31}P NMR (see the Supporting Information). These *in situ* formed catalysts had the same catalytic activity as that of isolated complexes **4** and **5** (entries 8–9). Varying the Lewis acid in the reaction demonstrated that while Cu(OTF) provided the desired product in good yield, the reaction time was greatly extended (entry 10). Other iron- or silver-based Lewis acids (entries 11–13) and non-redox Lewis acids such as Zn(OTf)$_2$, Sc(OTf)$_3$, and Yb(OTf)$_3$ (see the Supporting Information) failed to enable product formation. We also examined ligand **1** in catalysis, which lacks the boron Lewis acid, but it gave a much lower yield (entry 14), presumably due to the formation of lower concentrations of the active catalyst species. In addition, N-arylimidazole ligands [N-(2,6-diisopropylphenyl)-imidazole] that lack both the boron and 2-diphenylphosphino groups provide no product in the reaction (entry 15). Interestingly, the Pd(I) dimer (PtBu$_3$)Pd$_2$Br$_2$, which is known to perform ketone α-arylation reactions,[12] did form a small amount of product in the reaction (26%, entry 16).

Having established that bimetallic Pd catalysts provide optimal production of naphthalenes, we explored the substrate scope with respect to the aryl iodide coupling partner (Figure 4). For 4-substituted iodoarenes, we only observed a single isomer with the addition of two acetophenone molecules.
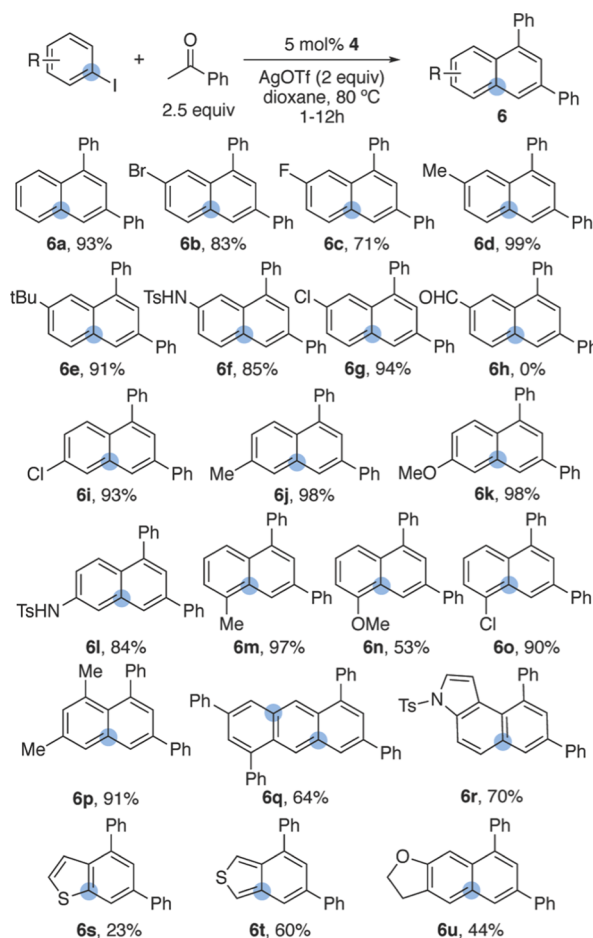

Figure 4. Aryl iodide substrate scope. Isolated yields of the product shown are for reactions run on a 0.5 mmol scale.

Thus, the 1,3-disubstituted naphthalene product contains a phenyl group beta to the carbon that originally contained the iodide (**6b**−**6g**). Aryl iodides containing substituents at either the meta- (**6i**−**6l**) or ortho-positions (**6m**−**6o**) also react to give the naphthalene products in high yields. Aryl iodides with meta-substituents also provided only a single observed regioisomer, where cyclization occurred at the less hindered position para to the substituent (**6i**−**6l**). Aldehyde functional groups were not tolerated in the reaction (**6h**), nor were cyanide or ester groups. Aryl bromides also did not lead to product formation. 1,4-Diiodobenzene gave the anthracene product in good yield via double cyclization (**6q**). Iodoheterocycles also provide annulation products. For example, 5-iodoindole gave the corresponding homologated product (**6r**) in high yield (70%). Other heterocycles, including 2- and 3-iodothiophenes provided the product in 23% (**6s**) and 60% (**6t**) yields, respectively, and 5-iododihydrobenzofuran gave the product in 44% yield (**6u**). With all aryl iodide substrates tested, only a single regioisomeric product was observed.

For the methyl ketone coupling partner (Figure 5), acetophenone derivatives containing both electron-rich and
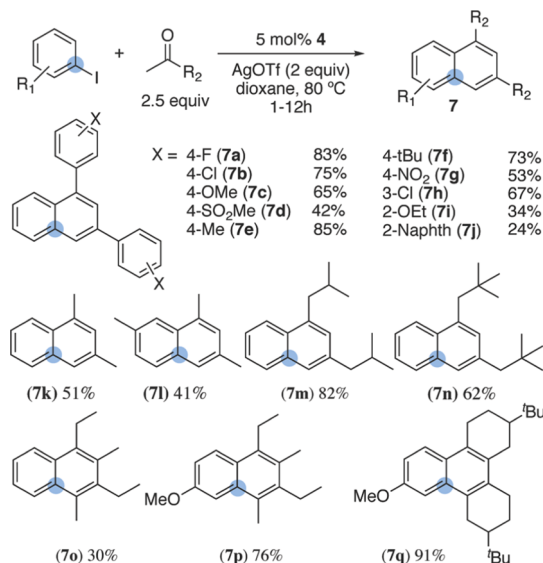

Figure 5. Methyl and dialkyl ketone substrate scope. Isolated yields of the product shown are for reactions run on a 0.5 mmol scale.

electron-poor aromatic rings perform well in the reaction (**7a**−**7j**). Substitution at the meta-position is well-tolerated (**7h**), but ortho-substituents lead to lower isolated yields (**7i** and **7j**). We also investigated the use of dialkyl ketones and found that acetone reacted to give the dimethylnaphthalene derivatives **7k** and **7l** in modest yields. More hindered ketones such as methyl isobutylketone gave higher yields of the products (**7m** and **7n**). We also tried 3-pentanone and found that the corresponding tetrasubstituted naphthalene could be isolated in modest yield with phenyl iodide (**7o**) but with much higher yield with 4-iodoanisole (**7p**). 4-*tert*-Butylcyclohexanone also reacted to give the tetrasubstituted naphthalene in excellent yield (91%, **7q**). This one step, regioselective synthesis of tetrasubstituted naphthalenes, provides access to core naphthalene structures that cannot be easily synthesized via other methods. Unfortunately, less hindered alkyl ketones such as 2-butanone gave complex mixtures of regioisomeric products.

To experimentally examine ketone incorporation, we performed the catalysis with simultaneous addition of two different ketones (Figure 6). Addition of 4-methoxy
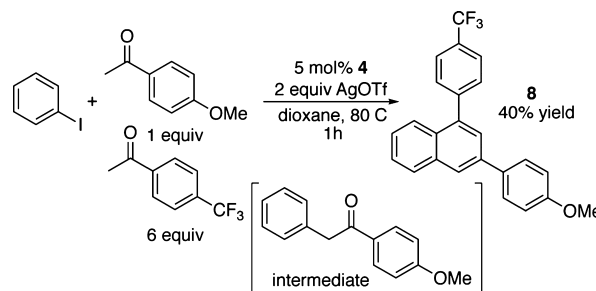

Figure 6. Heterocoupling selectivity in naphthalene synthesis.

acetophenone (1 equiv) and 4-trifluoromethyl acetophenone (6 equiv) to iodobenzene provided product **8** in 40% yield. The reaction required excess electron-deficient ketone because homocoupling with the more electron-rich ketone was observed as the major byproduct. With a 1:1 ratio of ketones, homocoupling of the more electron-rich ketone was the major product, and only an 18% yield of the heterocoupled product was observed. This suggests that the more electron-rich acetophenone undergoes addition to the aryl iodide at a faster rate than the more electron-deficient ketone. With the optimized number of ketone equivalents (6:1), the minor heterocoupled isomer (where trifluoromethylacetophenone was added first) was formed in only 6% yield, giving a 6.5:1 ratio of isomers.

With the demonstration that bimetallic Pd catalysts provide superior performance to monometallic Pd catalysts, we next executed DFT calculations and mechanistic experiments to outline possible reaction mechanisms and understand the reactivity and regioselectivity. First, we confirmed the necessity of the bimetallic Pd catalyst. When Pd is left out of the reaction (Table 1, entry 17), no product is observed. Also, added TfOH (2 equiv) shows no reaction conversion, indicating that a strong acid, such as TfOH, is unlikely to be generated and to induce cyclization (Table 1, entry 18). When the reaction of 4-chloroiodobenzene under standard conditions was stopped after 30 min at ∼50% conversion, we isolated the arylated ketone **9** as a major product (Figure 7a). This isolated intermediate is consistent with our hypothesis that the reaction proceeds via an initial bimetallic Pd-catalyzed ketone arylation reaction, followed by the addition of a second equivalent of ketone and then cyclization and aromatization. Indeed, we found that when 2-phenylacetophenone was subjected to the standard reaction conditions with 5 mol % catalyst **4**, product **6a** was isolated in 69% yield (Figure 7b). Interestingly, we also found that Pd catalyst **4** was necessary for the cyclization reaction to proceed efficiently as the reaction with 2-phenylacetophenone conducted without the Pd catalyst or with just ligand **3** gave only small amounts of the product (6% and 19% yield, respectively). This may indicate that the Pd catalyst participates in the cyclization event as well, potentially as a strong Lewis acid after chloride extraction with silver triflate. The addition of 1 equiv of TfOH to the cyclization shown in Figure 7b also did not impact the rate of formation of **6a**, suggesting that the TfOH generated in the reaction is not solely responsible for inducing the cyclization step (see the Supporting Information for conditions).
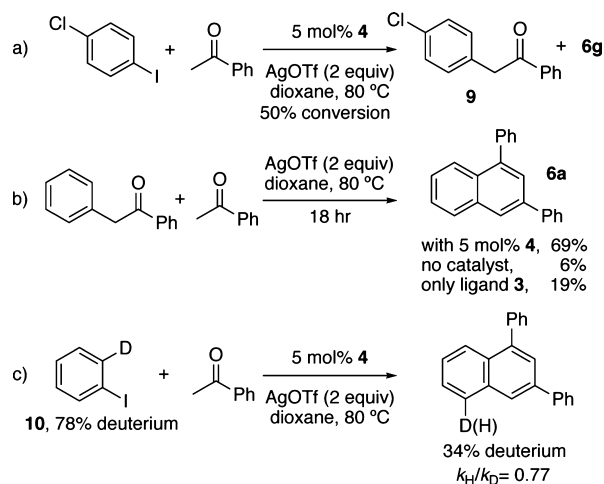
Figure 7. Mechanistic experiments (see the Supporting Information for reaction details).

enables sharing of the electronic burden of oxidation across two metal centers, similar to the scenario proposed by Ritter.[10]

To directly examine possible bimetallic Pd-catalyzed ketone α-arylation mechanisms, we used M06 DFT calculations with continuum or continuum/explicit 1,4-dioxane solvent. This functional provides the most generally accurate structures and energies for second–row transition metal complexes.[23] We generally modeled the bimetallic catalyst as structure **11** (Figure 8a) and phenyl iodide and methyl phenyl ketone as substrates.
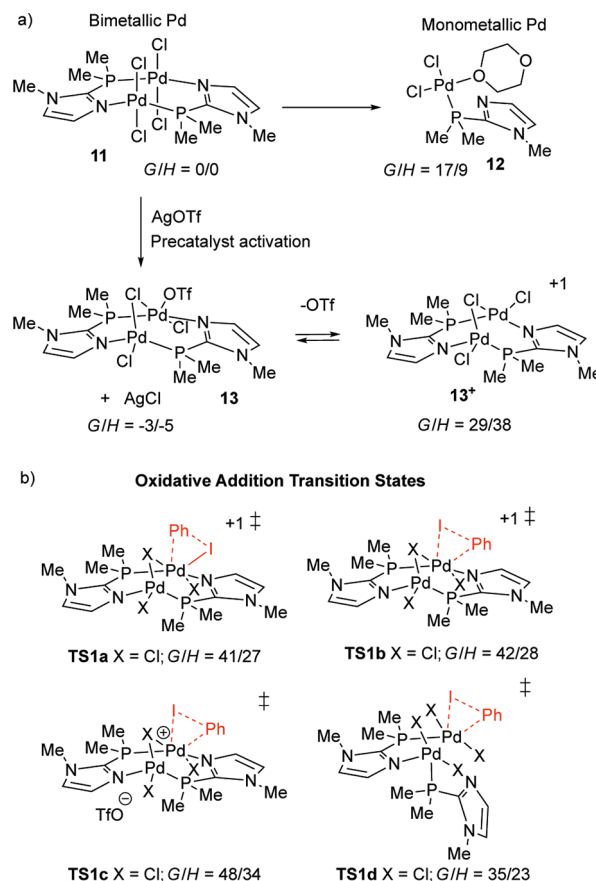

Figure 8. (a) DFT-calculated thermodynamic values for bimetallic Pd precatalyst conversion to a potential monometallic solvent complex and Ag-induced chloride dissociation. (b) Representative oxidative addition transition states. Catalyst phenyl groups were modeled as methyl groups. **TS1a** and **TS1b** energies relative to **13⁺**. **TS1c** energies relative to **13**. **TS1d** energies relative to **11**. Relative Gibbs energies (G) and enthalpies (H) are reported in kcal/mol.

We next conducted a kinetic isotope experiment to better understand the cyclization portion of the mechanism (Figure 7c). We synthesized *ortho*-deuteroiodobenzene (**10**) to perform a one-pot intramolecular competition experiment to determine the preference for the reaction to proceed via substitution of the hydrogen or deuterium atom. Based on the ratio of H/D in product naphthalene, we calculated a k_H/k_D of 0.77 in the reaction. This inverse secondary kinetic isotope effect suggests that the cyclization step of the reaction likely involves rehybridization of an sp^2 carbon, potentially through a Friedel−Crafts-type mechanism. There is also the possibility of the reaction proceeding through a 6-π-electrocyclic ring-closure mechanism if elimination of water occurs before cyclization. The inverse secondary isotope effect is also inconsistent with a rate-limiting Pd-mediated C−H activation event during cyclization.[25]

Typically, Pd-catalyzed α-arylations of ketones proceed under Pd(0)/Pd(II) catalysis in the presence of a base via oxidative addition into an aryl iodide.[26] Pd(I)-catalyzed α-arylations of carbonyl compounds also typically require stoichiometric formation of the enolate species with the base.[12] With bimetallic catalyst **4**, however, the reaction proceeds under relatively oxidizing conditions (2 equiv AgOTf; Ag$^+$ potential vs NHE = ~0.8 V), the addition of organic or inorganic bases (Et$_3$N, NaOtBu, and Cs$_2$CO$_3$) leads to the complete loss of reactivity, and no product or ketone arylation is observed. This suggests that one role of silver triflate may be to help facilitate enolization of the ketone in the absence of a strong base. We performed a deuterium exchange experiment and found that stoichiometric silver triflate facilitates deuterium transfer between deuterated and non-deuterated acetophenones at 80 °C in the absence of catalyst **4** (see the Supporting Information). We also examined the impact of oxygen on reactivity. There was no decrease in the rate or yield when the reaction to form **6a** was run under a balloon of oxygen at 80 °C. While this does not exclude the possibility of open-shell-type intermediates, it does suggest that the reaction does not proceed through a Pd(0)-to-Pd(II) catalytic cycle and likely occurs via higher-oxidation-state dimeric Pd(III) or Pd(IV) intermediates. This could explain why bimetallic catalysts **4** and **5** provide much higher yields in the reaction because the bimetallic structure of the catalyst

When bimetallic Pd complexes are used, there is always the possibility that the complex dissociates to form active monometallic catalysts. Therefore, we calculated the energy of transforming **11** into several possible monometallic structures, such as monometallic **12** (Figure 8a). The direct dissociation into a structure where each Pd center is ligated by a single 2-phosphinoimidazole requires $\Delta G/\Delta H$ = 37/54 kcal/mol. This relatively high energy is the result of the 2-phosphinoimidazole ligand only providing tight phosphine coordination and weak imidazole donation to a single Pd center, which is due to the P−C−N angle of 117° (Pd−P distance = 2.25 Å and Pd−N = 3.96 Å). Therefore, our best low-range estimate for bimetallic-to-monometallic conversion was obtained using an explicit dioxane solvent. The energy of

12 with explicit dioxane is $\Delta G/\Delta H$ = 17/9 kcal/mol higher than that of **11**. While this energy alone does not rule out the formation of reactive monometallic structures, the concentration of this type of species would be small. Moreover, in subsequent reaction steps, **12** would require more energy to achieve the oxidative addition (see later calculations). The poor simultaneous donation of both phosphine and imidazole ligand arms to a single Pd metal center explains the formation of **4** without Pd–Pd covalent bonding. Additionally, this suggests that the mixing of 2-phosphinoimidazole with PdCl$_2$ forms **4**.

With the inability of the starting bimetallic Pd complex to easily split into complete monometallic intermediates, we examined many other possible activation routes to generate reactive intermediates. We ruled out dimeric Pd(II)-to-Pd(I) reduction through Cl$_2$ reductive elimination that requires $\Delta G/\Delta H$ = 47/60 kcal/mol. We also examined the possibility that **11** acts as a one-electron donor to reduce phenyl iodide, but this requires >100 kcal/mol and is unlikely due to the low solvent polarity, although this value is overestimated due to the calculation of charge-separated species. Electron transfer from **11** to Ag$^+$ requires $\Delta G/\Delta H$ = 31/30 kcal/mol. It is unlikely that the phosphine ligand arm dissociates for **11** because even with the dioxane solvent stabilizing the coordination vacancy, this requires $\Delta G/\Delta H$ = 27/17 kcal/mol. The imidazole ligand arm, however, is more labile, requiring $\Delta G/\Delta H$ = 3/−7 kcal/mol for dissociation. This imidazole ligand arm dissociation could provide a monometallic-like reaction pathway while remaining as an overall bimetallic complex. Another reasonable activation pathway identified by calculations is chloride extraction from **11** to generate **13**$^+$ (Figure 8a). Starting from **11** and AgOTf, chloride for triflate anion exchange to form **13** is exergonic/exothermic with $\Delta G/\Delta H$ = −3/−5 kcal/mol, respectively. Generation of the cationic trichloride **13**$^+$ without an OTf anion coordination has $\Delta G/\Delta H$ = 29/38 kcal/mol, which suggests that the counterion, either the chloride or OTf anion, would remain in the outer solvation sphere. This also indicates that chloride and OTf anion exchange is likely very rapid under catalytic conditions. Importantly, both imidazole ligand arm dissociation and the thermodynamic accessibility of **13** and **13**$^+$ provide possible pathways for electrophilic-mediated substrate coordination and subsequent C–I bond activation.

To establish the general viability of the proposed bimetallic trichloride cationic complex, we synthesized the cationic BAr$^F_4$ salt **14** by treatment of complex **4** with 1 equiv of NaB(Ar^F)$_4$ [Figure 9a, Ar^F = 3,5-(CF$_3$)$_2$C$_6$H$_3$]. Importantly, the resulting isolated complex **14** is catalytically competent and has similar reactivity to that of complex **4**. In this X-ray structure and in the optimized DFT structure, one of the three chlorides provides a bridge to stabilize the vacant coordination site resulting from chloride dissociation (Figure 9b, the Pd–Pd distance is 2.772 Å).

To examine possible structures formed from the reaction of **4** with phenyl iodide, a stoichiometric amount of **4** was reacted with phenyl iodide and silver triflate. This allowed the isolation and X-ray structure of a bridging Pd–iodide species **15** with two triflate ligands (Figure 9b). The lack of isolation of a Pd–phenyl species is consistent with the DFT prediction that **16a** is relatively endergonic. The observation of this species, and the calculated thermodynamics for chloride to OTf anion ligand exchange indicate that chloride or OTf anions are possible as ancillary ligands during catalysis. More importantly,
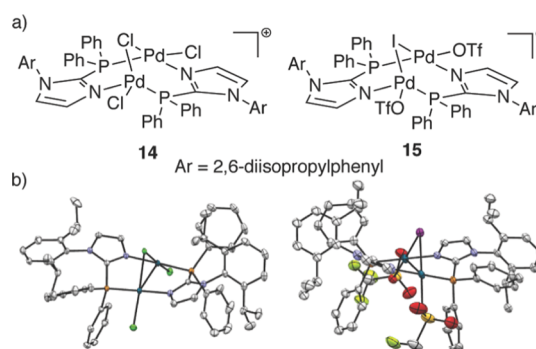

Figure 9. (a) Cationic bimetallic complexes containing bridging halides. (b) X-ray structures of complexes **14** and **15**. Anions {tetrakis[3,5-bis(trifluoromethyl)phenyl]borate for **14** and OTf for **15**} were omitted for clarity.

the presence of iodide in **15** suggests that oxidative addition/reductive elimination occurred under these conditions where the reductive elimination step produced phenyl chloride. This result is consistent with the work reported by Schoenebeck where halide exchange was shown to occur via an oxidative addition mechanism to the bimetallic Pd(I) complex.[12a] To confirm that the bridging species could be present during catalysis, we used mass spectrometry to examine the reaction mixture at the end of the reaction from entry 1 of Table 1. This confirmed the presence of an iodide-bridged bimetallic Pd complex (see the Supporting Information).

With both DFT and experiments indicating that a cationic bimetallic Pd intermediate is viable, we then calculated possible reactions between **13**$^+$ and phenyl iodide. We located exergonic π ($\Delta G/\Delta H$ = 4/−8 kcal/mol) and iodine σ ($\Delta G/\Delta H$ = 4/−9 kcal/mol) coordination intermediates. We identified two types of transition states for oxidative addition. **TS1a** connects the iodine-coordinated structure to the Pd(Ph)(I) oxidative addition intermediate through a 1,2-phenyl shift (Figure 8b). The second transition state located (**TS1b**) is the more expected three-centered oxidative addition process where Pd is inserted into the Ph–I bond. However, there is very little overall difference between the bonding in **TS1a** and **TS1b**, but there are subtle differences in bridging chlorides. The $\Delta G^{\ddagger}/\Delta H^{\ddagger}$ values for **TS1a** and **TS1b** are 41/27 and 42/28 kcal/mol, respectively. We extensively examined the possibility of the Ph–I bond being directly added across both Pd metal centers. However, the reduced dimensionality energy landscapes constructed only revealed the single metal center oxidative addition saddle point (see the Supporting Information). We also calculated the oxidative addition barrier with the OTf anion in an outer-sphere coordination of the second Pd metal center; however, the OTf anion remains close to the second Pd metal center at about 2.7 Å (**TS1c**; $\Delta G^{\ddagger}/\Delta H^{\ddagger}$ = 48/34 kcal/mol). Because our thermodynamic calculations suggest that chloride ligands can potentially be exchanged for OTf anion ligands, we also calculated the oxidative addition transition state with one or two chloride ligands replaced by OTf anions. Generally, we found that the activation barriers for one or two OTf ligands rather than chloride ligands are only a few kcal/mol higher in energy than the transition states shown in Figure 8b (see the Supporting Information). Therefore, it is not possible to be definitive about the chloride or OTf anion or a mixture coordinate to Pd metal centers during catalysis,

and we speculate that there is likely a mixture of active catalysts.

The oxidative addition transition state **TS1a** leads to the Pd−phenyl intermediate **16a** (Figure 10). In this intermediate,
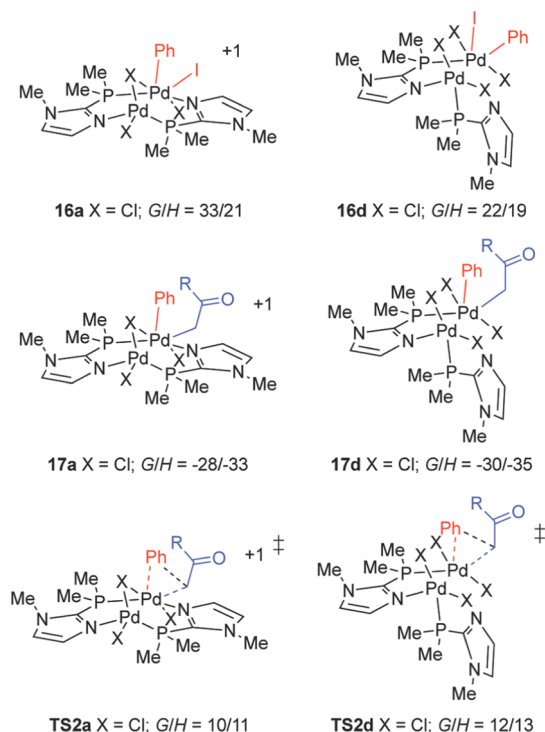

16a X = Cl; *G/H* = 33/21   **16d** X = Cl; *G/H* = 22/19

17a X = Cl; *G/H* = -28/-33   **17d** X = Cl; *G/H* = -30/-35

TS2a X = Cl; *G/H* = 10/11   **TS2d** X = Cl; *G/H* = 12/13

Figure 10. DFT-calculated energies for oxidative addition intermediates and reductive elimination (kcal/mol).

the halide ligands as well as the phenyl group are fluxional with only a 4 kcal/mol preference for the phenyl group to be *cis* compared to the second Pd metal center. In this cationic bimetallic pathway, the Pd−Pd distance progressively decreases. In neutral **13**, the Pd−Pd distance is 2.94 Å and decreases to 2.88 Å after chloride dissociation to **13$^+$**. At the oxidized intermediate, **16a**, the Pd−Pd distance is 2.72 Å. The significant decrease in the Pd−Pd distance suggests that the Pd(II) metal center likely donates electrons to the Pd(IV) metal center, creating a Pd(III)−Pd(III) bonding-type scenario.

While the oxidative addition activation barriers for **13$^+$** are potentially reasonable given the relatively elevated temperatures required for catalysis and experiments showing that anionic ligand exchange is possible, we also examined oxidative addition from neutral **13** with an imidazole ligand dissociated (**TS1d**). Somewhat surprisingly, this oxidative addition transition state has a lower barrier than **TS1a**, and this could suggest that anion exchange or anion ligand dissociation is a preequilibrium step. The oxidative addition barrier for **TS1d** has $\Delta G^{\ddagger}/\Delta H^{\ddagger}$ = 35/23 kcal/mol relative to **11**. This suggests that a more reactive species is generated through imidazole dissociation rather than chloride dissociation, although the energies of these pathways suggest that both mechanisms are viable for catalysis. Consistent with the idea that the bimetallic Pd complex **11** partly unravels, the resulting Pd−Ph intermediate, **16d**, with imidazole not coordinated is significantly lower in energy than a fully coordinated structure. The $\Delta G/\Delta H$ for **16d** is 17/28 kcal/mol, while re-coordination

of the imidazole raises the energy to $\Delta G/\Delta H$ = 34/48 kcal/mol. This indicates that the more donating Ph ligand creates a larger preference for imidazole ligand dissociation (and anion ligand dissociation).

Because the energy barriers for **TS1a** and **TS1d** are both within the margin of error for DFT-type calculations, we examined the rest of the catalytic cycle for both pathways. The relatively high oxidative addition barrier between **13$^+$** and the α-CH bond in methyl phenyl ketone (57/42 kcal/mol) indicates that the ketone does not react with Pd until after intermediate **16** is formed. The acidity of the α-CH bond in methyl phenyl ketone suggests that enolization provides a pathway to generate Pd−acyl intermediate **17** (Figure 10). While it is possible that Pd catalyzes ketone to enolate formation, deuterium exchange experiments described above using AgOTf show relatively rapid hydrogen−deuterium exchange between two different ketones. Therefore, the Pd−acyl intermediate can be achieved after AgOTf-induced enolization. From both intermediates **16a** and **16d** and Ag enolate, the halogen−ligand exchange reactions to give **17a** and **17d** are both exothermic by more than 30 kcal/mol. As expected, carbon coordination is ∼20 kcal/mol more stabilizing than oxygen enolate coordination.

The barrier for reductive elimination from **17a** to **TS2a** is $\Delta G^{\ddagger}/\Delta H^{\ddagger}$ = 10/11 kcal/mol and generates α-phenyl ketone as well as re-forms **13$^+$** (Figure 10). This reductive elimination occurs at a single Pd metal center. We also examined the possibility of reductive elimination where the Ph and acyl groups are on the opposite Pd metal centers. As with our efforts to identify oxidative addition across two Pd metal centers, we could not locate a transition state for this type of reaction route. For the imidazole-dissociated pathway, the reductive elimination barrier from **17d** to **TS2d** has $\Delta G^{\ddagger}/\Delta H^{\ddagger}$ = 12/13 kcal/mol, again similar to the cationic pathway barrier. After reductive elimination, it is lower in energy for the imidazole ligand arm to re-coordinate with the Pd metal center and re-form **11**.

Based on our experimental and computational evaluations, Figure 11 outlines two plausible bimetallic Pd catalytic cycles and subsequent cyclization. The catalytic cycle shown in Figure 11a involves conversion of **4** into an active cationic bimetallic Pd catalyst **19** through Ag-mediated chloride abstraction. The cycle begins with oxidative addition at a single Pd metal center to generate a Pd(III)−Pd(III)−phenyl intermediate containing a relatively strong metal−metal interaction (**20**). This intermediate can be considered a Pd(III) dimer because the Pd−Pd bond distance (2.72 Å for **16a**) is within the distance for Pd−Pd bond formation. Subsequent enolization and transmetalation facilitated by Ag generate a bimetallic Pd−acyl intermediate (**21**) where reductive elimination forms the α-arylation product **22** and reforms the cationic bimetallic Pd intermediate. It is likely that both the chloride and OTf anion-ligated species can promote catalysis in this cycle. Figure 11b shows a potentially competitive catalytic cycle with **4** undergoing imidazole ligand arm dissociation to generate the coordinatively unsaturated bimetallic active species **23**. Oxidative addition generates a Pd(IV)−Ph intermediate that is not directly stabilized by the second Pd(II) metal center (Pd−Pd distance = 3.99 Å). Subsequent transmetalation and reductive elimination generate **22**. The α-arylation process in the formation of naphthalene products explains the observed regioselectivity in the reaction. After ketone α-arylation, a non-catalytic route to the naphthalene product involves the
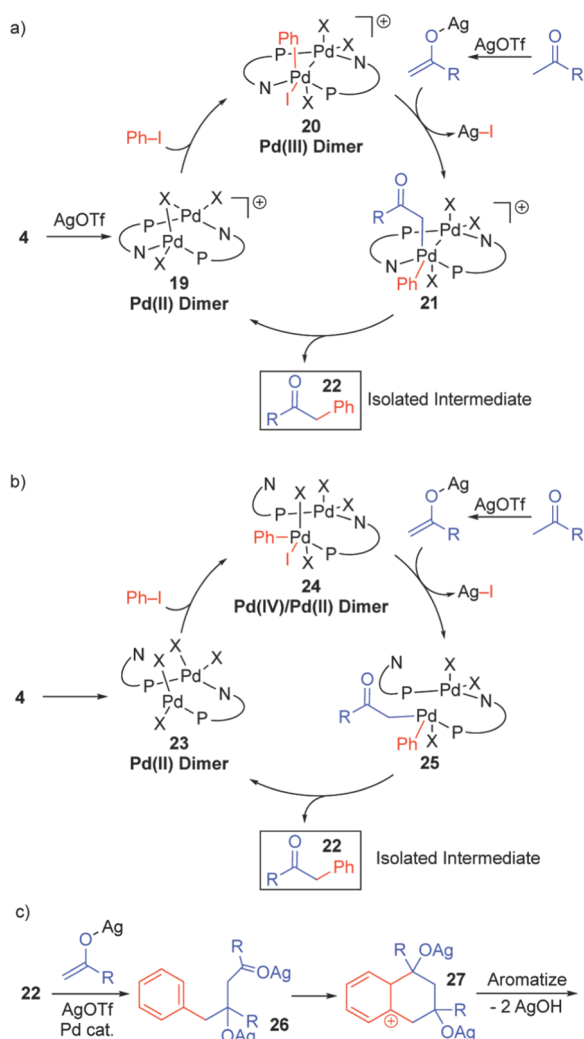
Figure 11. Possible catalytic cycles based on experimental and DFT results. (a) Bimetallic catalytic cycle involving cationic structures and a Pd(III)−Pd(III) intermediate. (b) Bimetallic catalytic cycle involving neutral structures, imidazole ligand arm dissociation, and a Pd(IV)−Pd(II) intermediate. (c) Mechanism of 1,3-naphthalene formation.

addition of a second equivalent of the enolate to intermediate **22** via an aldol condensation that would then provide **26** (Figure 11c). Friedel−Crafts-type cyclization by the attack of the arene ring onto the pendant ketone then gives intermediate **27**. Aromatization (via formal loss of AgOH) then occurs to give naphthalene product **6**.

We selected three different monometallic models to compare to these bimetallic catalytic cycles. These include the monometallic Pd complex from the dissociation of **11** [(2-phosphinoimidazole)PdCl₂], (imidazole)(PMe₃)PdCl₂, and (dppe)PdCl₂. The (imidazole)(PMe₃)PdCl₂ complex was examined because the monometallic structures formed from **11** are likely not a good direct comparison since there is strong phosphine coordination but weak imidazole coordination, which is very different bonding than that observed in the fully intact bimetallic complex.

We first calculated the barriers for oxidative addition of these model monometallic complexes. Not surprisingly, because 2-phosphinoimidazole provides poor imidazole coordination to a single Pd metal center, the formation of fully monometallic (2-

phosphinoimidazole)PdCl₂ is highly endothermic. For [(2-phosphinoimidazole)PdCl]⁺, oxidative addition with phenyl iodide only requires $\Delta G^{\ddagger}/\Delta H^{\ddagger}$ 21/8 kcal/mol. This indicates that while the monometallic catalyst is potentially highly reactive, ground-state accessibility inhibits catalysis through this type of dimer-to-monomer pathway. Somewhat surprisingly, the oxidative addition transition state energies for [(imidazole)(PMe₃)PdCl]⁺ and [(dppe)PdCl]⁺ with phenyl iodide require $\Delta G^{\ddagger}/\Delta H^{\ddagger}$ = 20/6 and $\Delta G^{\ddagger}/\Delta H^{\ddagger}$ = 26/11 kcal/mol, respectively. Because these oxidative addition barriers are relatively low, especially compared to **TS1a** and **TS1d**, these types of cationic monometallic structures are likely thermodynamically inaccessible. Indeed, calculation of AgOTf-mediated chloride extraction shows that it requires >40 kcal/mol to generate these cationic structures. This implies that one major feature of the Pd bimetallic catalysis reported here is the balance of generating reactive intermediates and the subsequent ability of these intermediates to achieve oxidative addition.

■ CONCLUSIONS

We have demonstrated that bimetallic 2-phosphinoimidazole-derived Pd(I) and Pd(II) complexes enable the formation of di- and tetrasubstituted naphthalene derivatives via a ketone α-arylation/cyclization process. This new transformation provides easy and efficient access to substituted naphthalenes from aryl iodides and methyl ketones and tolerates a range of functional groups at the aryl iodide and methyl ketone partners. DFT calculations and experiments were carried out to examine possible reaction mechanisms and understand the exceptional reactivity of our bimetallic catalysts. Two plausible catalytic cycles emerged. The first involves the generation of a cationic bimetallic intermediate, followed by oxidative addition to form a Pd(III)−Pd(III)-like intermediate and then transmetalation and reductive elimination. In the second and lower in energy pathway (although within the error of DFT calculations), catalysis can potentially occur through oxidative addition with the neutral catalyst to generate a bimetallic Pd(IV)−Pd(II) intermediate, which can also subsequently undergo transmetalation and reductive elimination to generate the initial α-arylation product. Ag-induced annulation forms the final naphthalene products.

■ ASSOCIATED CONTENT

ⓈI Supporting Information

The Supporting Information is available free of charge at https://pubs.acs.org/doi/10.1021/acscatal.1c02731.

> Experimental procedures, characterization data, spectral images, computational details, and calculated energies (PDF)
>
> XYZ coordinates of key structures (XYZ)
>
> X-ray crystallographic data for Pd(I) dimer **5** (CIF)
>
> X-ray crystallographic data for Pd(II) dimer **4** (CIF)
>
> X-ray crystallographic data for bridging iodide dimer **15** (CIF)
>
> X-ray crystallographic data for bridging chloride BArF₄ dimer **14** (CIF)

■ AUTHOR INFORMATION

Corresponding Authors

Daniel H. Ess − *Department of Chemistry and Biochemistry, Brigham Young University, Provo, Utah 84602, United*

States; ![orcid](https://orcid.org/0000-0001-5689-9762); Email: dhe@chem.byu.edu

David J. Michaelis − *Department of Chemistry and Biochemistry, Brigham Young University, Provo, Utah 84602, United States;* ![orcid](https://orcid.org/0000-0003-3914-5752); Email: dmichaelis@chem.byu.edu

Authors

Chloe C. Ence − *Department of Chemistry and Biochemistry, Brigham Young University, Provo, Utah 84602, United States*

Erin E. Martinez − *Department of Chemistry and Biochemistry, Brigham Young University, Provo, Utah 84602, United States*

Samuel R. Himes − *Department of Chemistry and Biochemistry, Brigham Young University, Provo, Utah 84602, United States*

S. Hadi Nazari − *Department of Chemistry and Biochemistry, Brigham Young University, Provo, Utah 84602, United States*

Mariur Rodriguez Moreno − *Department of Chemistry and Biochemistry, Brigham Young University, Provo, Utah 84602, United States*

Manase F. Matu − *Department of Chemistry and Biochemistry, Brigham Young University, Provo, Utah 84602, United States*

Samantha G. Larsen − *Department of Chemistry and Biochemistry, Brigham Young University, Provo, Utah 84602, United States*

Kyle J. Gassaway − *Department of Chemistry and Biochemistry, Brigham Young University, Provo, Utah 84602, United States*

Gabriel A. Valdivia-Berroeta − *Department of Chemistry and Biochemistry, Brigham Young University, Provo, Utah 84602, United States*

Stacey J. Smith − *Department of Chemistry and Biochemistry, Brigham Young University, Provo, Utah 84602, United States*

Complete contact information is available at:
https://pubs.acs.org/10.1021/acscatal.1c02731

Notes

The authors declare no competing financial interest.

◼ REFERENCES

(1) (a) Farley, C. M.; Uyeda, C. Organic Reactions Enabled by Catalytically Active Metal-Metal bonds. *Trends Chem.* **2019**, *1*, 497−509. (b) Powers, I. G.; Uyeda, C. Metal−Metal Bonds in Catalysis. *ACS Catal.* **2017**, *7*, 936−958. (c) Pye, D. R.; Mankad, N. P. Bimetallic Catalysis for C−C and C−X Coupling Reactions. *Chem. Sci.* **2017**, *8*, 1705−1718. (d) Cooper, B. G.; Napoline, J. W.; Thomas, C. M. Catalytic Applications of Early/Late Heterobimetallic

Complexes. *Catal. Rev.* **2012**, *54*, 1−40. (e) Ritleng, V.; Chetcuti, M. J. Hydrocarbyl Ligand Transformations on Heterobimetallic Complexes. *Chem. Rev.* **2007**, *107*, 797−858.

(2) Nakamura, E.; Yoshikai, N.; Yamanaka, M. Mechanism of C-H Bond Activation/C-C Bond Formation Reaction Between Diazo Compound and Alkane Catalyzed by Dirhodium Tetracarboxylate. *J. Am. Chem.* **2002**, *124*, 7181−7192.

(3) (a) Mazzacano, T. J.; Mankad, N. P. Base Metal Catalysts for Photochemical C-H Borylation That Utilize Metal-Metal Cooperativity. *J. Am. Chem. Soc.* **2013**, *135*, 17258−17261. (b) Leon, N. J.; Yu, H.-C.; Mazzacano, T. J.; Mankad, N. P. Pursuit of C−H Borylation Reactions with Non-Precious Heterobimetallic Catalysts: Hypothesis-Driven Variations on a Design Theme. *Synlett* **2020**, *31*, 125−132.

(4) (a) Cammarota, R. C.; Lu, C. C. Tuning Nickel with Lewis Acidic Group 13 Metalloligands for Catalytic Olefin Hydrogenation. *J. Am. Chem. Soc.* **2015**, *137*, 12486−12489. (b) Ramirez, B. L.; Sharma, P.; Eisenhart, R. J.; Gagliardi, L.; Lu, C. C. Bimetallic Nickel-Lutetium Complexes: Tuning the Properties and Catalytic Hydrogenation Activity of the Ni Site by Varying the Lu Coordination Environment. *Chem. Sci.* **2019**, *10*, 3375−3384. (c) Ramirez, B. L.; Lu, C. C. Rare-Earth Supported Nickel Catalysts for Alkyne Semihydrogenation: Chemo- and Regioselectivity Impacted by the Lewis Acidity and Size of the Support. *J. Am. Chem. Soc.* **2020**, *142*, 5396−5407.

(5) (a) Zhou, Y.-Y.; Uyeda, C. Catalytic Reductive [4 + 1]-Cycloadditions of Vinylidenes and Dienes. *Science* **2019**, *363*, 857−862. (b) Pal, S.; Zhou, Y.-Y.; Uyeda, C. Catalytic Reductive Vinylidene Transfer Reactions. *J. Am. Chem. Soc.* **2017**, *139*, 11686−11689. (c) Pal, S.; Uyeda, C. Evaluating the Effect of Catalyst Nuclearity in Ni-Catalyzed Alkyne Cyclotrimerizations. *J. Am. Chem. Soc.* **2015**, *137*, 8042−8045.

(6) (a) Inatomi, T.; Koga, Y.; Matsubara, K. Dinuclear Nickel(I) and Palladium(I) Complexes for Highly Active Transformations of Organic Compounds. *Molecules* **2018**, *23*, 140. (b) Zhou, W.; Napoline, J. W.; Thomas, C. M. A Catalytic Application of Co/Zr Heterobimetallic Complexes: Kumada Coupling of Unactivated Alkyl Halides with Alkyl Grignard Reagents. *Eur. J. Inorg. Chem.* **2011**, 2029−2033.

(7) (a) Tsutsumi, H.; Sunada, Y.; Shiota, Y.; Yoshizawa, K.; Nagashima, H. Nickel(II), Palladium(II), and Platinum(II) η3-Allyl Complexes Bearing a Bidentate Titanium(IV) Phosphinoamide Ligand: A Ti←M₂ Dative Bond Enhances the Electrophilicity of the π-Allyl Moiety. *Organometallics* **2009**, *28*, 1988−1991. (b) Walker, W. K.; Anderson, D. L.; Stokes, R. W.; Smith, S. J.; Michaelis, D. J. Allylic Aminations with Hindered Secondary Amine Nucleophiles Catalyzed by Heterobimetallic Ti−Pd Complexes. *Org. Lett.* **2015**, *17*, 752−755. (c) Walker, W. K.; Kay, B. M.; Michaelis, S. A.; Anderson, D. L.; Smith, S. J.; Ess, D. H.; Michaelis, D. J. Origin of Fast Catalysis in Allylic Amination Reactions Catalyzed by Pd−Ti Heterobimetallic complexes. *J. Am. Chem. Soc.* **2015**, *137*, 7371−7378. (d) Ence, C. C.; Walker, W. K.; Stokes, R. W.; Martinez, E. E.; Sarager, S. M.; Smith, S. J.; Michaelis, D. J. Synthesis of Chiral Titanium-Containing Phosphinoamide Ligands for Enantioselective Heterobimetallic Catalysis. *Tetrahedron* **2019**, *75*, 3341−3347.

(8) Parmelee, S. R.; Mazzacano, T. J.; Zhu, Y.; Mankad, N. P.; Keith, J. A. A Heterobimetallic Mechanism for C−H Borylation Elucidated from Experimental and Computational Data. *ACS Catal.* **2015**, *5*, 3689−3699.

(9) Powers, D. C.; Ritter, T. Bimetallic Redox Synergy in Oxidative Palladium Catalysis. *Acc. Chem. Res.* **2012**, *45*, 840−850.

(10) (a) Powers, D. C.; Ritter, T. Bimetallic Pd(III) Complexes in Palladium-Catalyzed Carbon−Heteroatom Bond Formation. *Nat. Chem.* **2009**, *1*, 302−309. (b) Powers, D. C.; Lee, E.; Ariafard, A.; Sanford, M. S.; Yates, B. F.; Canty, A. J.; Ritter, T. Connecting Binuclear Pdᴵᴵᴵ and Mononuclear Pdᴵⱽ Chemistry by Pd-Pd Bond Cleavage. *J. Am. Chem. Soc.* **2012**, *134*, 12002−12009. (c) Canty, A. J.; Ariafard, A.; Sanford, M. S.; Yates, B. F. Mechanism of Pd-Catalyzed Ar−Ar Bond Formation Involving Ligand-Directed C−H Arylation and Diaryliodonium Oxidants: Computational Studies of Orthopalladation at Binuclear Pd(II) Centers, Oxidation To Form

Binuclear Palladium(III) Species, and Ar···Ar Reductive Coupling. *Organometallics* **2013**, *32*, 544−555. (d) Powers, D. C.; Ritter, T. A Transition State Analogue for the Oxidation of Binuclear Palladium-(II) to Binuclear Palladium(III) Complexes. *Organometallics* **2013**, *32*, 2042−2045.

(11) Xu, W.; Li, M.; Qiao, L.; Xie, J. Recent Advances of Dinuclear Nickel- and Palladium-Complexes in Homogeneous Catalysis. *Chem. Commun.* **2020**, *56*, 8524−8536.

(12) (a) Hama, T.; Ge, S.; Hartwig, J. F. Palladium-Catalyzed α-Arylation of Zinc Enolates of Esters: Reaction Conditions and Substrate Scope. *J. Org. Chem.* **2013**, *78*, 8250−8266. (b) Hama, T.; Hartwig, J. F. α-Arylation of Esters Catalyzed by the Pd(I) Dimer {[P(t-Bu)₃]PdBr}₂. *Org. Lett.* **2008**, *10*, 1545−1548. (c) Bercot, E. A.; Caille, S.; Bostick, T. M.; Ranganathan, K.; Jensen, R.; Faul, M. M. Diastereoselective Palladium-Catalyzed α-Arylation of 4-Substituted Cyclohexyl Esters. *Org. Lett.* **2008**, *10*, 5251−5254. (d) Hama, T.; Culkin, D. A.; Hartwig, J. F. Palladium-Catalyzed Intermolecular α-Arylation of Zinc Amide Enolated under Mild Conditions. *J. Am. Chem. Soc.* **2006**, *128*, 4976−4985.

(13) (a) Bonney, K. J.; Proutiere, F.; Schoenebeck, F. Dinuclear Pd(I) Complexes−Solely Precatalysts? Demonstration of Direct Reactivity of a Pd(I) Dimer with an Aryl Iodide. *Chem. Sci.* **2013**, *4*, 4434−4439. (b) Fricke, C.; Sperger, T.; Mendel, M.; Schoenebeck, F. Catalysis with Palladium(I) Dimers. *Angew. Chem., Int. Ed.* **2021**, *60*, 3355−3366.

(14) (a) Díez, V.; Espino, G.; Jalón, F. A.; Manzano, B. R.; Pérez-Manrique, M. Synthesis and Structure of New Palladium Complexes with the Ligand 2-(Diphenylphosphino)-1-Methylimidazole: Evidence of Hemilability. *J. Organomet. Chem.* **2007**, *692*, 1482−1495. (b) Done, M. C.; Rüther, T.; Cavell, K. J.; Kilner, M.; Peacock, E. J.; Braussaud, N.; Skelton, B. W.; White, A. Novel Cationic and Neutral Pd(II) Complexes Bearing Imidazole Based Chelate Ligands: Synthesis, Structural Characterisation and Catalytic Behaviour. *J. Organomet. Chem.* **2000**, *607*, 78−92. (c) Abdul Jalil, M.; Yamada, T.; Fujinami, S.; Honjo, T.; Nishikawa, H. An Imidazole-Based P−N Bridging Ligand and its Binuclear Copper(I), Silver(I) and Palladium(I) Complexes: Synthesis, Characterizations and X-ray Structures. *Polyhedron* **2001**, *20*, 627−633.

(15) For recent examples, see: (a) Hein, S. J.; Lehnherr, D.; Arslan, H.; J Uribe-Romo, F.; Dichtel, W. R. Alkyne Benzannulation Reactions for the Synthesis of Novel Aromatic Architectures. *Acc. Chem. Res.* **2017**, *50*, 2776−2788. (b) Yu, L.-Z.; Wei, Y.; Shi, M. Synthesis of Polysubstituted Polycyclic Aromatic Hydrocarbons by Gold-Catalyzed Cyclization−Oxidation of Alkylidenecyclopropane-Containing 1,5-Enynes. *ACS Catal.* **2017**, *7*, 4242−4247. (c) Yadav, S.; Hazra, R.; Singh, A.; Ramasastry, S. S. V. Substituent-Guided Palladium-Ene Reaction for the Synthesis of Carbazoles and Cyclopenta[b]indoles. *Org. Lett.* **2019**, *21*, 2983−2987. (d) Dal Zotto, C.; Wehbe, J.; Virieux, D.; Campagne, J.-M. FeCl₃-Catalyzed Intramolecular Hydroarylation of Alkynes. *Synlett* **2008**, *1*, 2033−2035. (e) Kabalka, G. W.; Ju, Y.; Wu, Z. A New Titanium Tetrachloride Mediated Annulation of α-Aryl-Substituted Carbonyl Compounds with Alkynes: A Simple and Highly Efficient Method for the Regioselective Synthesis of Polysubstituted Naphthalene Derivatives. *J. Org. Chem.* **2003**, *68*, 7915−7917.

(16) Makar, S.; Saha, T.; Singh, S. K. Naphthalene, A Versatile Platform in Medicinal Chemistry: Sky-High Perspective. *Eur. J. Med. Chem.* **2019**, *161*, 252−276.

(17) Mulembo, T.; Nagai, G.; Tamagawa, H.; Nitta, T.; Sasaki, M. Conductive and Flexible Multi-Walled Carbon Nanotube/Polydimethylsiloxane Composites Made with Naphthalene/Toluene Mixture. *J. Appl. Polym. Sci.* **2019**, *136*, 48167−48175.

(18) Shudo, Y.; Karim, M. R.; Ohtani, R.; Nakamura, M.; Hayami, S. Hybrids From the π-π Stacking of Graphene Oxide and Aromatic Sulfonic Compounds for Improved Proton Conductivity. *ChemElectroChem* **2018**, *5*, 238−241.

(19) Martinez, E. E.; Jensen, C. A.; Larson, A. J. S.; Kenney, K. C.; Clark, K. J.; Nazari, S. H.; Valdivia-Berroeta, G. A.; Smith, S. J.; Ess, D. H.; Michaelis, D. J. Monosubstituted, Anionic (Imidazolyl) N-

Heterocyclic Carbene Complexes of Palladium and Their Activity in Cross-Coupling Reactions. *Adv. Synth. Catal.* **2020**, *362*, 2876−2881.

(20) Johansson Seechurn, C. C. C.; Sperger, T.; Scrase, T. G.; Schoenebeck, F.; Colacot, T. J. Understanding the Unusual Reduction Mechanism of Pd(II) to Pd(I): Uncovering Hidden Species and Implications in Catalytic Cross-Coupling Reactions. *J. Am. Chem. Soc.* **2017**, *139*, 5194−5200.

(21) (a) Chipman, J. A.; Berry, J. F. Paramagnetic Metal−Metal Bonded Heterometallic Complexes. *Chem. Rev.* **2020**, *120*, 2409−2447. (b) Cordero, B.; Gómez, V.; Platero-Prats, A. E.; Revés, M.; Echeverría, J.; Cremades, E.; Barragán, F.; Alvarez, S. Covalent radii revisited. *Dalton Trans.* **2008**, *21*, 2832−2838. (c) Dong, H.; Meng, Q.; Chen, B.-Z.; Wu, Y.-B. Theoretical studies on the multiple metal-metal bonds in the bimetallic molecules and the ultrashort V-Mn bonds in the complexes. *J. Organomet. Chem.* **2012**, *717*, 108−115.

(22) (a) Addison, A. W.; Rao, T. N.; Reedijk, J.; Van Rijn, J.; Verschoor, G. C. Synthesis, Structure, and Spectroscopic Properties of Copper(II) Compounds Containing Nitrogen-Sulfur Donor Ligands: The Crystal and Molecular Structure of Aqua[1,7-bis(N-methyl-benzimidazol-2'-yl)-2,6-dithiaheptane]copper(II) Perchlorate. *J. Chem. Soc., Dalton Trans.* **1984**, *7*, 1349−1356. (b) Okuniewski, A.; Rosiak, D.; Chojnacki, J.; Becker, B. Coordination polymers and molecular structures among complexes of mercury(II) halides with selected 1-benzoylthioureas. *Polyhedron* **2015**, *90*, 47−57. (c) Yang, L.; Powell, D. R.; Houser, R. P. Structural Variation in Copper(I) Complexes with Pyridylmethylamide Ligands: Structural Analysis with a New Four-coordinate Geometry Index, τ4. *Dalton Trans.* **2007**, *9*, 955−964.

(23) Frisch, M. J.; Trucks, G. W.; Schlegel, H. B.; Scuseria, G. E.; Robb, M. A.; Cheeseman, J. R.; Scalmani, G.; Barone, V.; Petersson, G. A.; Nakatsuji, H.; Li, X.; Caricato, M.; Marenich, A. V.; Bloino, J.; Janesko, B. G.; Gomperts, R.; Mennucci, B.; Hratchian, H. P.; Ortiz, J. V.; Izmaylov, A. F.; Sonnenberg, J. L.; Williams; Ding, F.; Lipparini, F.; Egidi, F.; Goings, J.; Peng, B.; Petrone, A.; Henderson, T.; Ranasinghe, D.; Zakrzewski, V. G.; Gao, J.; Rega, N.; Zheng, G.; Liang, W.; Hada, M.; Ehara, M.; Toyota, K.; Fukuda, R.; Hasegawa, J.; Ishida, M.; Nakajima, T.; Honda, Y.; Kitao, O.; Nakai, H.; Vreven, T.; Throssell, K.; Montgomery, J. A., Jr.; Peralta, J. E.; Ogliaro, F.; Bearpark, M. J.; Heyd, J. J.; Brothers, E. N.; Kudin, K. N.; Staroverov, V. N.; Keith, T. A.; Kobayashi, R.; Normand, J.; Raghavachari, K.; Rendell, A. P.; Burant, J. C.; Iyengar, S. S.; Tomasi, J.; Cossi, M.; Millam, J. M.; Klene, M.; Adamo, C.; Cammi, R.; Ochterski, J. W.; Martin, R. L.; Morokuma, K.; Farkas, O.; Foresman, J. B.; Fox, D. J. *Gaussian 16*, Rev. B.01; Gaussian Inc.: Wallingford, CT, 2016. (b) Zhao, Y.; Truhlar, D. G. The M06 Suite of Density Functionals for Main Group Thermochemistry, Thermochemical Kinetics, Noncovalent Interactions, Excited States, and Transition Elements: Two New Functionals and Systematic Testing of Four M06-class Functionals and 12 Other Functionals. *Theor. Chem. Acc.* **2008**, *120*, 215−241.

(24) (a) All structures were reoptimized from the starting crystal structure with the M06 functional using the 6-31G**[LANL2DZ for Pd] basis set in Gaussian 16. Structures were confirmed as minima or transition states by vibrational frequency analysis. Reported enthalpies correspond to 298 K and 1 atm using the standard thermochemistry corrections in Gaussian 16. The SMD solvent model for dioxane was used in all calculations. (b) Marenich, A. V.; Cramer, C. J.; Truhlar, D. G. Universal Solvation Model Based on Solute Electron Density and on a Continuum Model of the Solvent Defined by the Bulk Dielectric Constant and Atomic Surface Tensions. *J. Phys. Chem. B* **2009**, *113*, 6378−6396.

(25) Park, H.; Yoo, K.; Jung, B.; Kim, M. Direct Synthesis of Anthracenes from o-Tolualdehydes and Aryl Iodides through Pd(II)-Catalyzed sp³ C−H Arylation and Electrophilic Aromatic Cyclization. *Tetrahedron* **2018**, *74*, 2048−2055.

(26) (a) Culkin, D. A.; Hartwig, J. F. Palladium-Catalyzed α-Arylation of Carbonyl Compounds and Nitriles. *Acc. Chem. Res.* **2003**, *36*, 234−245. (b) Stradiotto, M. Ancillary Ligand Design in the

Development of Palladium Catalysts for Challenging Selective Monoarylation Reactions. *RSC Catal. Ser.* **2015**, *21*, 228−253.